

Using the AIMS™ 45-193i for hyper-NA imaging applications

Peter De Bisschop^{*a}, Vicky Philipsen^a,
Robert Birkner^b, Ute Buttgerit^b, Rigo Richter^b, Thomas Scherübl^b
^aIMEC, Kapeldreef 75, B-3001 Leuven, Belgium;
^bCarl Zeiss SMS GmbH, Carl Zeiss Promenade 10, 07745 Jena, Germany

ABSTRACT

We have tested the validity of the so-called ‘vector-effect emulation mode’ of the newest member of the AIMS™¹ family, the AIMS™ 45-193i, that was recently developed for Hyper-NA applications. This vector-effect emulation mode (also called ‘scanner mode’) converts the measured signals into a prediction of what the image-in-resist of a Hyper-NA scanner would be (so including vector- and polarization effects). We’ve done a number of experiments that directly test the validity of this vector-effect emulation, by comparing them to rigorous lithographic simulations and to CD-measurements from printed NA=1.20 scanner wafers, and found that the AIMS™ 45-193i results are in fact quite accurate. Afterwards we looked at a number of potential Hyper-NA imaging applications for the AIMS™ 45-193i, again comparing it to rigorous simulations and wafer CD-measurements. These results indicate that, next to its traditional use as reticle-inspection tool, the AIMS™ 45-193i has potential use also in the wafer fab as an ‘imaging-inspection’ or ‘OPC-defect inspection’ tool, especially when applied to 2D patterns.

Keywords: AIMS, Hyper-NA imaging, vector-effect emulation, OPC

1. INTRODUCTION

The use of AIMS™ for e.g. reticle-defect detection or inspection after repair has become a standard in many mask shops for a long time now². An AIMS™ system uses the same reticle-illumination conditions as the scanner for which the reticle is intended to be used and the lens of the AIMS™ also has the same NA as the scanner. The lens of an AIMS™ system, however, makes a magnified image of the reticle-area that is being illuminated, so that this image can be captured with a CCD camera. This means that whereas the reticle-side of the AIMS™ is equivalent to the scanner, the image side is not: due to the high (e.g. ×450) image-magnification, the angles-of-incidence in the image plane are very small, and hence the image is essentially a scalar image: vector- and polarization-effect virtually play no role. This is very different with the image formation in a hyper-NA scanner, where the angles-of-incidence in the resist are large, such that vector- and polarization effects are very important indeed. The scalar-image of the AIMS™ is therefore very different from the vector-image of a scanner, and as-measured AIMS™ images are not equivalent to scanner images at hyper-NA imaging conditions .

This has changed with the introduction of the AIMS™ 45-193i^(3,4). This tool was developed for the 45 nm node on a completely new platform, and it is equipped with a so-called ‘vector-effect emulator’, which ‘converts’ the actually measured (scalar) AIMS™ images into a prediction of the image-in-resist of the scanner, given a certain index-of-refraction of the (assumed) resist and of the immersion-fluid. (Thin-film effects are not included in the emulation.) See also Figure 1.

The AIMS™ 45-193i can be operated in two modes:

- The ‘AIMS mode’, where the system is set to generate the original, scalar images only. This is the ‘traditional’ type of AIMS™ operational mode: the vector-effect emulator is not being used.
- The ‘Scanner mode’: the vector-effect emulation mode *is* being used now, and the images now incorporate vector- and polarization effects and should be equivalent to scanner image-in-resist.

Both operational modes include the possibility to capture the images through focus. In the case of the ‘scanner mode’, the focus scale is converted into the appropriate scanner focus scale, too.

* peter.debisschop@imec.be, phone +32 16 281314

The ‘scanner mode’, though being more time consuming than the ‘AIMS mode’, offers the benefit of providing a more relevant image of a reticle defect (or any reticle structure), since it is intended to correspond to the image-in-resist in the scanner.

Question then of course, is to assess how accurately this ‘vector-effect emulator’ succeeds in predicting these ‘scanner-mode’ images: they are not the results of a direct measurement, but a combination of actual image-measurements (in ‘AIMS mode’) and Zeiss-proprietary software, ‘converting’ the measured image-intensity data into this ‘scanner-mode image’.

The goal of this paper is twofold.

- First we have done a few experiments with which we wanted to test the validity of this vector-effect emulation mode. These experiments were designed such that the outcome was known from first principles or could be compared to the results of rigorous lithography simulations and wafer CD-measurement in cases that are not too much affected by details of the ‘experimental’ settings, such as resist effects. We will see that the accuracy of the vector-effect emulation could indeed be confirmed for the test cases considered in this paper.
- Next we explored a few possible ‘imaging-applications’ of the ‘scanner mode’ of the AIMS™ 45-193i, i.e. experiments from which we try to learn something about hyper-NA lithographic imaging. We looked at e.g. measurement of Exposure Latitude (EL), MEF and through-focus behavior of simple Line-Space (L/S) structures, as well as lithographic performances of 2D structures. Also here, we will compare results from the ‘scanner mode’ with rigorous lithography simulations and CD-measurements from wafers printed on a hyper-NA scanner. Goal of this second part was to assess possible use of the AIMS™ 45-193i in the wafer fab., i.e. imaging-related applications of the system, as an extension of the more ‘traditional’ use of AIMS™ for reticle-defect review and inspection.

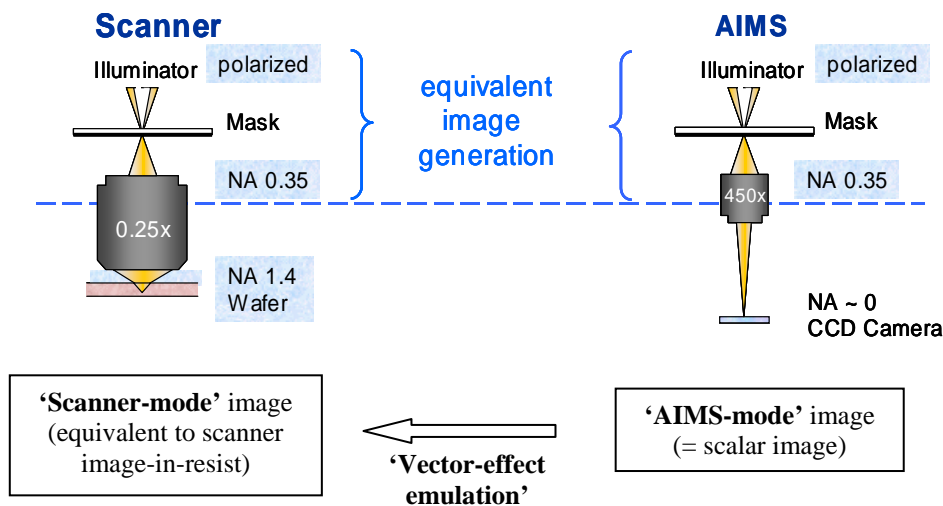


Fig. 1. Comparison of the operation of an AIMS™ system with a wafer scanner. At reticle-side, both systems are equivalent, but the AIMS™ uses a magnifying lens, whereas the scanner demagnifies. The result is that as-measured AIMS™ images are basically ‘scalar’ images. The ‘vector-effect emulator’ used in the so-called ‘scanner mode’ of the new AIMS™45-193i, however, ‘converts’ the as-measured images into a ‘scanner-equivalent’ image, i.e. into a prediction of the image-in-resist in the scanner.

2. VALIDATION OF THE ‘VECTOR-EFFECT EMULATION’ MODE

We have done two types of experiments to test the validity of the ‘vector-effect emulation’ mode of the AIMS™ 45-193i. The first test looks for the zero image-contrast pitch under TM-polarization. The second considers the optimum π -space bias for minimizing 0- π space imbalance in alternating PSM L/S imaging.

1.1 Zero contrast

Applying the AIMS™ 45-193i for predicting image-in-resist contrast has already been done before³. We extended this work by doing contrast measurements around the pitch for which the image contrast is expected to be zero. It is well known that this can occur for L/S imaging, in case of two-beam imaging, if the illumination polarization used is TM. For the simple two-beam imaging case, the image contrast will be zero if the angle Θ between the two beams in the imaging medium is 90° (see figure 2a), which can be shown to occur at the pitch given by the following approximate formula

$$P_{ZeroContrast} \approx \frac{\lambda}{\sqrt{2} n_2} \quad (1)$$

where λ is the illuminating wavelength and n_2 the index-of-refraction of the medium in which the image is evaluated. In resist, having a typical refractive index of 1.7, the resulting zero-contrast pitch is ~ 80 nm, a pitch that was not available on the test mask we used in the experiment. To test this zero-contrast case experimentally on the AIMS™ 45-193i, we therefore evaluated the image contrast in water ($n_2 = 1.44$), for which the zero-contrast pitch as given by equation (1) becomes 95 nm. Using a X-polarized DipoleX35 $\sigma = 0.98/0.774$ (σ -outer/ σ -inner) setting and NA = 1.16 on the AIMS™ 45-193i, and specifying a refractive index of 1.44 (both for immersion fluid *and* resist) in the vector-effect emulation, we measured the ‘scanner images’ for L/S pitches of 90 to 100 nm in steps of 1 nm.

A Solid-E simulation at these settings (see figure 2b) gives a more precise value of the zero-contrast pitch than equation (1), and also illustrates that for pitches lower than this value, the contrast should reverse. The goal of the experiment is therefore not only to find the zero contrast, but also to observe this contrast reversal.

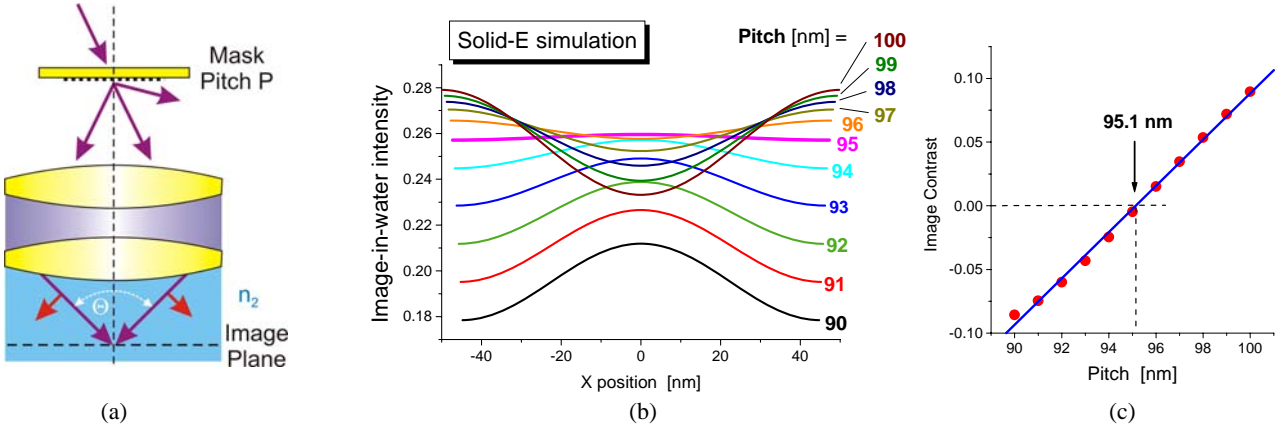


Fig. 2. Zero-contrast experiment: prediction

(a): illustration of a TM-polarized two-beam imaging case (equivalent to zero-pole size Dipole illumination)

(b) and (c): Solid-E simulation of the image-in-water ($n_2 = 1.44$) and derived image contrast, for NA = 1.16, DipoleX35, $\sigma = 0.98/0.774$, X-polarized, 6% attenuated PSM (The substrate was also given the optical properties of water, i.e. $n = 1.44$ and $k = 0$. The absorber mask line-width was taken as $Pitch/2$)

Figure 3 shows the result of the experiment. It is instructive to compare the image-intensities in the ‘scanner mode’ to the ‘AIMS™-mode’ signals, taken from the same mask structures under identical conditions. The ‘AIMS™-mode’ signals show a high image contrast for all pitches, as could be expected because of the scalar imaging in this case. The ‘scanner-mode’ signals however have the expected low contrast, with zero contrast between pitch 95 and 96 nm (i.e. very close to the expected value), and contrast reversal for pitches below 95 nm. This result is a nice confirmation of the validity of

the ‘vector-effect emulation’, as the low contrast is not at all present in the signals that are actually measured, but had to be entirely ‘reconstructed’ by the vector-effect emulator.

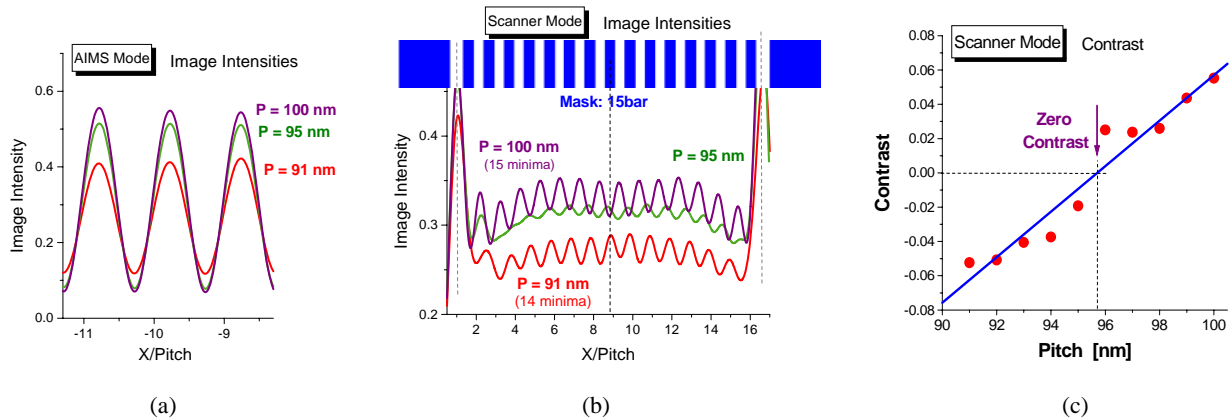


Fig. 3 Zero-contrast experiment: results obtained on the AIMS™45-193i (using a binary Cr mask)

- (a): measured image intensities for 3 pitches, obtained in the ‘AIMS™ mode’, i.e. *without* applying the vector emulation
- (b): measured image-intensities over the 15-bar L/S structure, for 3 pitches in ‘Scanner mode’, i.e. *with* the vector-effect emulator applied. Clearly visible is the close-to-zero contrast at pitch = 95 nm, and the inverted contrast at the 91 nm pitch
- (c): measured image contrast vs. pitch obtained in the ‘scanner mode’, i.e. now with the vector-effect emulation applied. The zero-contrast point is correctly observed between 95 and 96 nm pitch.

1.2 Space imbalance for L/S structures on an alternating PSM mask

A second experiment we intended as an explicit test of the vector-effect emulation mode is related to the well-known “ $0-\pi$ space imbalance”⁵ that can occur when printing L/S patterns with an alternating phase-shift mask (alt.PSM). If the width of the $0-$ and π -space on the mask (i.e. the non-phase shifted and phase-shifted space between the absorber lines) are drawn to have equal width, mask-3D effects induce a contrast imbalance between the two spaces in the image, which in turn leads to an apparent displacement of the resist lines in the image. This type of line-position error can be avoided if a π -space bias (B) is applied to the mask, i.e. the $0-$ and π -space are not drawn at equal width, but differ by an amount B. This bias must then be chosen such that the image contrast in both spaces is equal again. Figure 4 illustrates this contrast-imbalance phenomenon. As the value of the optimum bias is due to a primarily optical effect (and has little dependence on e.g. the resist being used), comparing the ‘best bias’ obtained from image-intensity measurements on the AIMS™ 45-193i with CD-measurements from wafers printed on a hyper-NA scanner, provides a convenient second test case in this study.

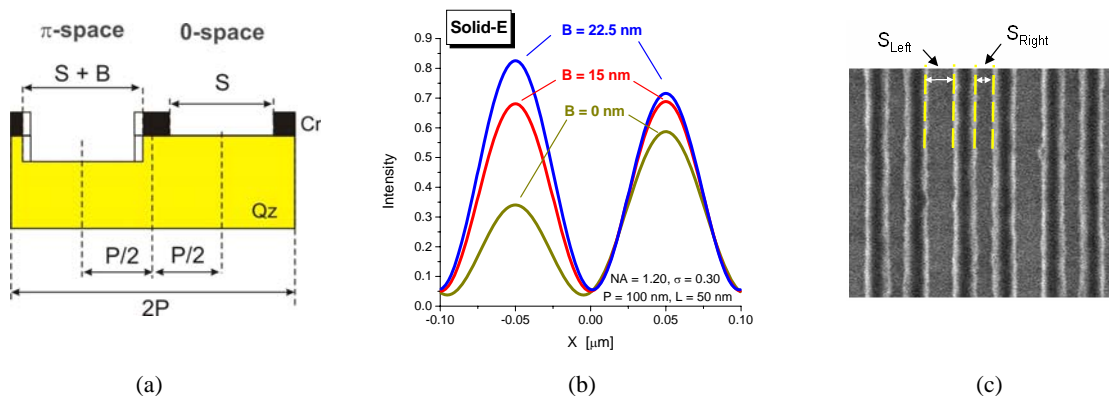


Fig. 4. Illustration of the $0-\pi$ space imbalance phenomenon

- (a): mask cross section, illustrating the definition of nomenclature used
- (b): Solid-E simulation of image-in-resist intensity, for several values of the $0-\pi$ space width bias, B
- (c): example of a top-down SEM picture of the printed L/S pattern, in a case where B is not well optimized.

In the experiment we used an alt.PSM mask on which 12 bias values B are available. We took ‘scanner-mode’ AIMSTM 45-193i images for all 12 bias cases, in order to find the optimum value of B for which the contrast imbalance would be \sim zero. The same mask was then exposed on an ASML XT:1700i scanner, and determined the optimum bias from top-down SEM measurements of the ‘Space_Imbalance’ ΔS , which is defined as

$$\text{Space_Imbalance} \equiv \Delta S \equiv S_{\text{Left}} - S_{\text{Right}} \quad (2)$$

The optimum π -space bias corresponds to $\Delta S \approx 0$.

Figures 5a and 5b show the result of these two optimum-bias determinations, for the case of a 120 nm pitch L/S pattern exposed at NA = 1.20 unpolarized $\sigma = 0.3$ conventional setting. Both the intensity-imbalance results from the AIMSTM 45-193i, as well as the space-imbalance measurements from the printed wafer indicate that the optimum bias is just below 20 nm. So again, we find an excellent agreement. Interestingly, the value of the optimum bias as determined from a Solid-E simulation is \sim 15 nm, as can be seen in figure 4b. Even though the cause for this discrepancy between the simulated and measured value of the optimum bias is currently not well understood, it is likely that it is due to some deviation between the actual mask and its idealized version that is being used in the simulation. This further underlines the benefit AIMSTM using the actual mask, including all its real properties, and not relying on some idealized model of the mask. (Note that we also did a similar comparison for a 160 nm pitch, now taking an NA = 0.85, with the same good agreement.)

The experiment was taken one step further by considering also the focus-dependency of the space-imbalance, $\Delta S(F)$. (Note that the space-imbalance can also be calculated from the AIMS intensities by applying an appropriate threshold.) Around best focus, the $\Delta S(F)$ dependency is linear, so that we can characterize it by the slope $d\Delta S/dF$. Figure 5c makes an additional AIMS-scanner comparison, now using this $d\Delta S/dF$ quantity. Again, the agreement is good.

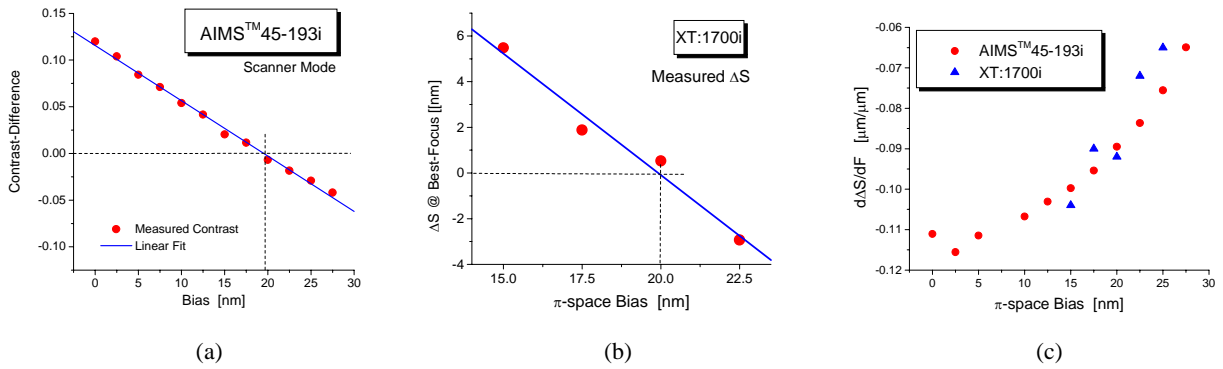


Fig. 5 0- π space imbalance: Experimental results (120 nm pitch L/S pattern; NA = 1.20)

- (a): AIMSTM 45-193i (scanner mode): 0- π space contrast difference vs. π -space bias B (at best focus)
- (b): XT:1700i space-imbalance, ΔS , vs. π -space bias B (at best focus)
- (c): $d\Delta S/dF$ (focus dependency of ΔS) comparing AIMSTM 45-193i with XT:1700i wafer data.

3. IMAGING APPLICATIONS FOR SIMPLE L/S STRUCTURES

The results from the previous section confirm the validity of the ‘vector-effect emulation’ mode of the AIMSTM 45-193i for the test cases we considered. We now continue this study by exploring a few other potential imaging applications of this system. This means that we continue to use the ‘scanner mode’, but now use the system to measure lithographic quantities like EL, MEF, through-focus performance and optical proximity. Again we will place the AIMSTM 45-193i results next to XT:1700i wafer-measurement data, but as the absolute values of the quantities considered now have a non-negligible impact from e.g. the resist-process used, we cannot consider these comparisons as true validation tests any more. These tests are now rather exploring possible wafer-fab applications of the AIMSTM 45-193i, in which the system is used for screening lithographic quantities (e.g. trends), without needing to expose wafers. One could consider this type of experiment as having a position being in between rigorous simulations, where the reticle is usually assumed

to be perfect, and results from real wafers exposures, where the results will be impacted by any known or unknown imperfection of the reticle. Therefore, an AIMS™ 45-193i could be used in the wafer fab for imaging-related ‘screening’ experiments, and hence reduce the actual scanner and wafer-metrology time needed to optimize certain mask- or scanner-related settings. The examples shown in this section only provide a selection of the experiments that could be done in this way.

1.3 Exposure Latitude (EL)

CD-values can be derived from the image intensities measured by the AIMS™ 45-193i by applying some appropriate image-intensity threshold, and from the dependency of this CD on the threshold value, an Exposure Latitude can be calculated. This EL-value is based on image-intensities only and does not incorporate any effect of the resist, so one cannot expect an agreement of the absolute value of an EL measured from AIMS™ 45-193i data with the EL obtained from comparable wafer-exposure data. But it is of interest to see whether at least the trends would agree. If this is the case, AIMS™ 45-193i experiments could help e.g. in EL-optimization exercises.

Figure 6a shows a comparison of the maximum EL vs. pitch data for 6% attenuated PSM (MoSi) L/S structures. The comparison includes AIMS™ 45-193i data, measurements from XT:1700i scanner wafers and Solid-E image-in-resist simulations (all for NA = 1.20 cQuad20 $\sigma = 0.97/0.84$ XY-polarized settings). We indeed see similar trends in the EL(pitch) dependency between these three data sets, but no agreement between the absolute values. We already mentioned the effect of the resist as one of the reasons for differing absolute values between the wafer-CD data and the image-based data. The reason why the AIMS™ results also differ from the Solid-E simulation results are less easy to attribute, although potential candidates include reticle-imperfections, imperfections of the AIMS™ 45-193i lens, etc.

Figure 6b shows another AIMS™ 45-193i vs. XT:1700i wafer-CD data maximum-EL comparison, this time as a correlation plot between the two data sets. The data was now taken from different mask types (including standard types, such as 6% attenuated PSM and binary Cr masks, but also ‘alternative mask stacks’ such as thick-Cr binary, and two Ta/SiO₂ attenuated PSM stacks) as well as different pitches. Once again we find that the absolute values differ, the more interesting observation is that both data sets correlate well. This demonstrates the potential of the AIMS™ 45-193i system for EL-optimization. The fact that the data of figure 6b includes measurements from different mask stacks provides an additional confirmation that AIMS™ 45-193i correctly captures mask-3D effects.

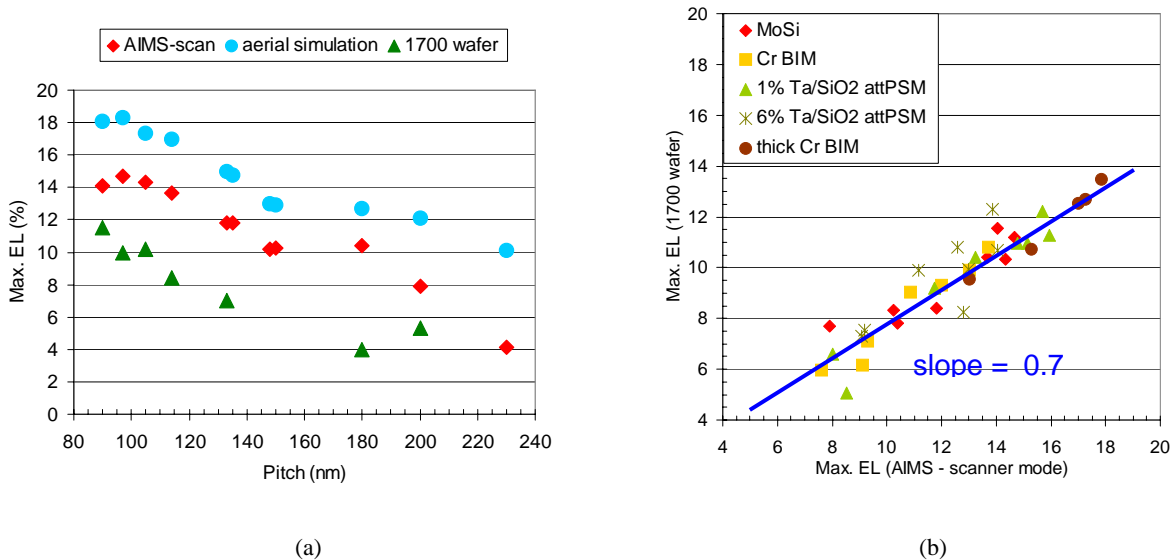


Fig. 6 Maximum Exposure Latitude (NA = 1.20, cQuad20 $\sigma = 0.97/0.84$)

- (a): 6% att.PSM (MoSi) mask: comparison between data from AIMS™ 45-193i (scanner mode), XT:1700i wafer data and Solid-E image-in-resist simulations
- (b): AIMS™ 45-193i (scanner mode) vs. XT:1700i wafer-CD data, for various mask stacks and pitches

1.4 Mask-Error Factor (MEF)

We measured the MEF for several L/S patterns on a 6% attenuated PSM (MoSi) and binary (Cr) mask, comparing again the results obtained from the AIMS™ 45-193i with CD-data from wafers printed on the XT:1700i immersion scanner, and with Solid-E image-in-resist simulations. The settings used were $NA = 1.20$, $cQuad20 \sigma = 0.97/0.84$, XY-polarized.

Figure 7 shows the results for the case of the MoSi mask. The MEF-values obtained from the AIMS™ 45-193i measurements agree very well with the Solid-E image-in-resist calculations, confirming that the AIMS™ 45-193i correctly captures the purely optical (including mask 3D) effects. The MEF values obtained from the XT:1700i wafers are systematically higher, but this is due to the ‘resist-contribution’ of the MEF values, which is of course not present in the AIMS™ results.

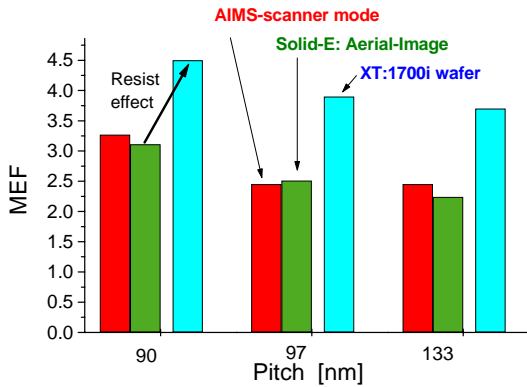


Fig. 7 Comparison of MEF-values for attenuated PSM L/S structures ($NA = 1.20$, $cQuad20 \sigma = 0.97/0.84$, XY-polarized).

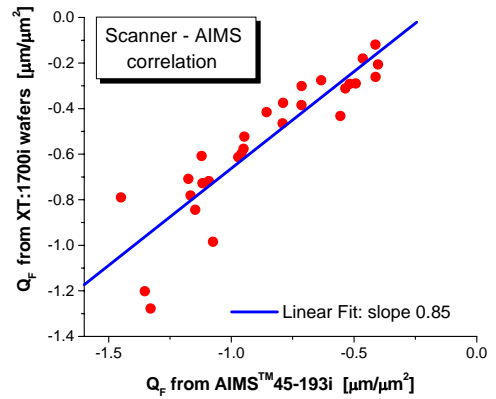


Fig. 8 Correlation of the quadratic-focus sensitivity factor, Q_F , for attenuated PSM L/S structures with SRAF, comparing results from the AIMS™ 45-193i with CD data from wafers printed on a XT:1700i scanner. ($NA = 1.20$, Annular $\sigma = 0.96/0.72$, XY-polarized)

1.5 Through-focus behavior

The last lithographic figure-of-merit we looked at is the through-focus (F) behavior. Every AIMS™ 45-193i measurement captures images through focus (focus-interval and step-size specified by the user), and therefore automatically yields CD(F) results. This can then again be compared to through-focus CD data obtained from printed wafers, using the same mask and illumination settings.

Instead of measuring complete process windows and extract Depth-of-Focus (DOF), we used a simpler metric that can be measured from a CD(F) curve at a single dose (or image-threshold). CD(F) curves usually fit quite well to a parabola, i.e. we can fit the CD data with the following formula

$$CD(F) = CD_0 + Q_F (F - F_0)^2 \quad (3)$$

The fit parameter Q_F represents the curvature of the parabolic fit; we call it the ‘quadratic focus sensitivity’ of the particular litho structure being considered, at the dose (or image threshold) for which the CD(F) data were obtained. Q_F is expressed in $\mu\text{m}/\mu\text{m}^2$ units; its value is ~ 0 for a structure-dose combination that is close to iso-focal behavior (e.g. 1:1 dense L/S structures). For most L/S structures with larger pitch, Q_F is usually negative.

We have used this Q_F metric to make a comparison of the through-focus behavior of a series of L/S patterns, each with some Sub-Resolution Assist-Feature (SRAF) rule applied, comparing again the AIMS™ 45-193i with the results from wafers printed on our XT:1700i scanner. Experimental settings were $NA = 1.20$, Annular $\sigma = 0.96/0.72$ illumination, XY-polarized; we used a 6% attenuated PSM mask (MoSi).

Figure 8 shows a correlation plot between the Q_F values obtained with the AIMS™ 45-193i vs. Q_F values measured from XT:1700i wafers (all L/S structures with different SRAF rules). We find a result similar to what we've seen before (e.g. when making similar comparisons EL and MEF values): we do observe a good correlation but the absolute values do not agree. And again, we can refer to e.g. the impact of the resist to explain this difference of the absolute values. The existence of good correlation, however, means that one could use AIMS™ 45-193i data to e.g. compare the effectivity of different SRAF rules, or – more in general – the relative DOF performance of different litho structures.

4. IMAGING APPLICATIONS FOR 2D STRUCTURES

In the previous section we saw that AIMS™ 45-193i image-data can correctly predict trends or relative values for important lithographic quantities like Exposure Latitude, MEF and through-focus CD behavior. Of course, as long as we consider simple 1D litho structures, the prediction of trends or the optimization of some mask or scanner parameter is more easily done by rigorous simulations than by AIMS™ experiments. Parameters can be easily and quickly changed in the simulator, the calculation throughput is quite high and there is no need to actually build a mask, which also makes it cheaper. So as a 'competitor' of lithographic simulators, AIMS™ 45-193i has a number of drawbacks when we think only of simple L/S structures.

Several of these arguments change, however, once we move to more complicated and/or large scale structures. Rigorous simulators cannot handle larger mask areas and including mask-3D effects – increasingly important at hyper-NA - becomes very difficult if not practically impossible (due to calculation-time and memory constraints) for many structures.

The AIMS™ 45-193i, however, does not have the same constraints, on the contrary. Every measurement captures the image intensity in a $\sim 10 \times 10 \mu\text{m}$ area (at 4X), at different focus levels. The user can decide afterwards, i.e. when analyzing the results, where exactly in the image he wants to make a CD evaluation. The AIMS™ 45-193i analysis software automatically generates Bossung-type data for this structure (at a user-selected image threshold). From the previous experiments, we have seen that the 'scanner mode' of the AIMS™ 45-193i seems to take correct account of mask-3D and polarization effects, and the measurements are of course based on the actual mask and not on some idealized version of it that one usually considers in simulators. All this seems to make the 'scanner mode' of the AIMS™ 45-193i a natural tool to explore and inspect the lithographic performance of more complicated and/or larger-area mask structures, from the actual mask itself.

Figure 9 illustrates these arguments for the example of a (still rather simple) 2D structure. The image was measured at 7 focus-positions around 'best focus' (automatically detected in the AIMS™ 45-193i as the image that has the largest overall contrast). As all these images are saved, the user can afterwards (when doing off-line analysis) decide on a certain position he wants to analyze. In the example of Figure 9 we chose to analyze the CD of the gap between the two horizontally oriented line ends. The off-line software then automatically displays (and outputs) the corresponding image-intensity cuts, and – for a user-specified image-threshold value – the corresponding Bossung data (lower-right graph). The selected threshold value can also be used to extract image-intensity contours from the entire image (lower-left graph).

We have also done an initial comparison between these AIMS™ 45-193i data for small 2D structures and data from a wafer printed on the XT:1700i scanner. We compared i) contours extracted from the AIMS™ 45-193i image intensities with top-down SEM images from the corresponding wafer prints, ii) CD measurements of a selected gap in the 2D structure and iii) Exposure latitude of this gap. In total we looked at eighteen 2D structures, belonging to the three different structure types that are illustrated in figure 10. For the analysis of the AIMS™ 45-193i data we used a single image threshold for all 18 structures, i.e. we did not recalibrate the threshold for every structure individually.

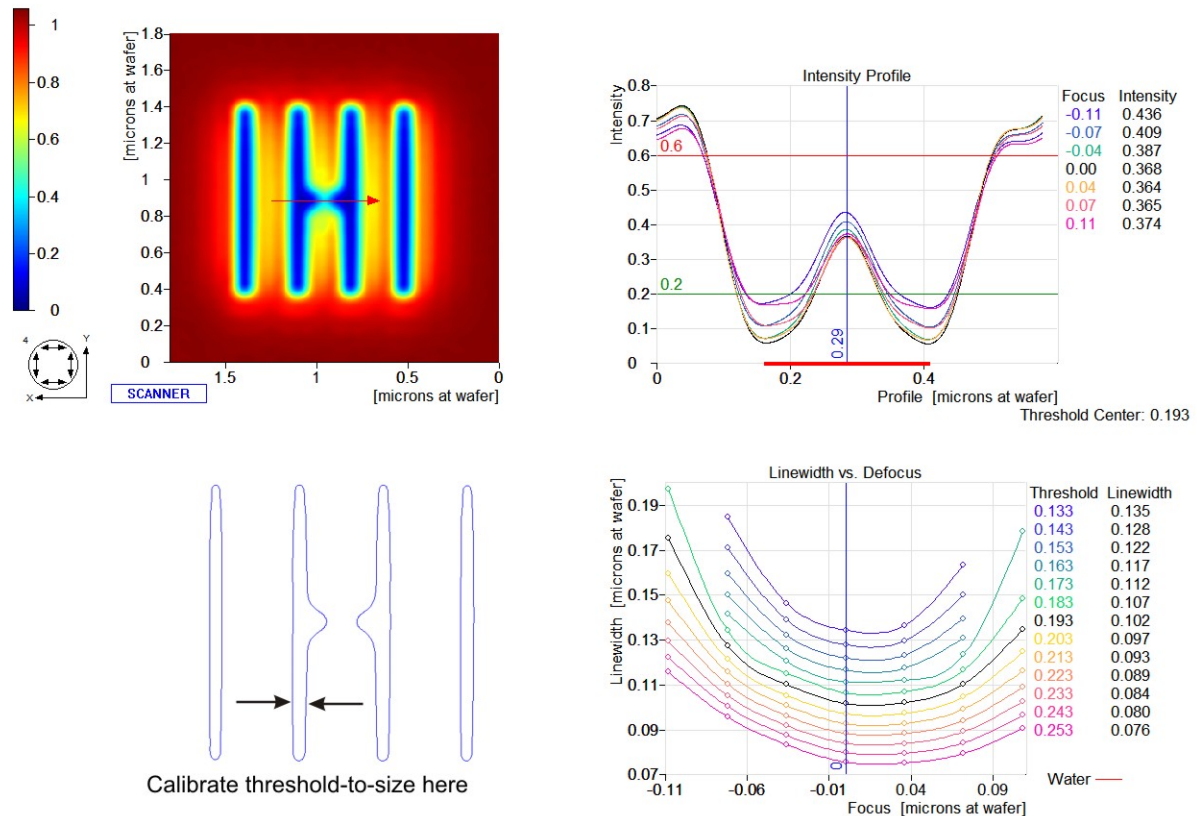


Fig. 9 Example of AIMS™ 45-193i images and off-line analysis results for a small 2D structure. The lower-left contour-image shows where on the vertical line segment the threshold-to-size was determined to match the line-CD obtained from a printed XT:1700i wafer, exposed at the same conditions. This threshold-to-size value was then used to generate the Bossung (lower-right) and contour (lower-left). (NA = 1.20 Annular $\sigma = 0.96/0.72$ XY-polarized)

The images of figure 10a show an overlay of the SEM image with the AIMS™ 45-193i contours. The agreement is quite satisfactory, but of course this type of comparing the results from the two measurements is not very quantitative. Figure 10b compares the measured CD of the gap (marked with a line) in each of the images. For some structures the agreement is remarkably good, for others there seems to be an offset. As we argued earlier, this should not surprise us, as the AIMS™ 45-193i data does not incorporate any effect of the resist-process.

For the same reason, we cannot expect the absolute EL values to agree. More interesting from a practical point of view, however, is the correlation plot of the EL data in figure 10c. As in case of the L/S structures (see figure 6b) we find a reasonable correlation between the two EL-data sets. This suggests that the AIMS™ 45-193i can be used to generate reliable EL-trend trends, and could therefore e.g. be used to inspect points in a larger layout where e.g. a critical EL is suspected. A potential application for the AIMS™ 45-193i would therefore be to use it for inspection of critical EL-areas in complicated 2D patterns, in the same way as some OPC packages do this today: a user-defined EL-threshold could flag critical or failing sites in the 2D pattern.

One can assume that a similar use for through-focus performance could also be made.

In the summary, we will further comment on the type of practical applications that present themselves from the results we obtained here.

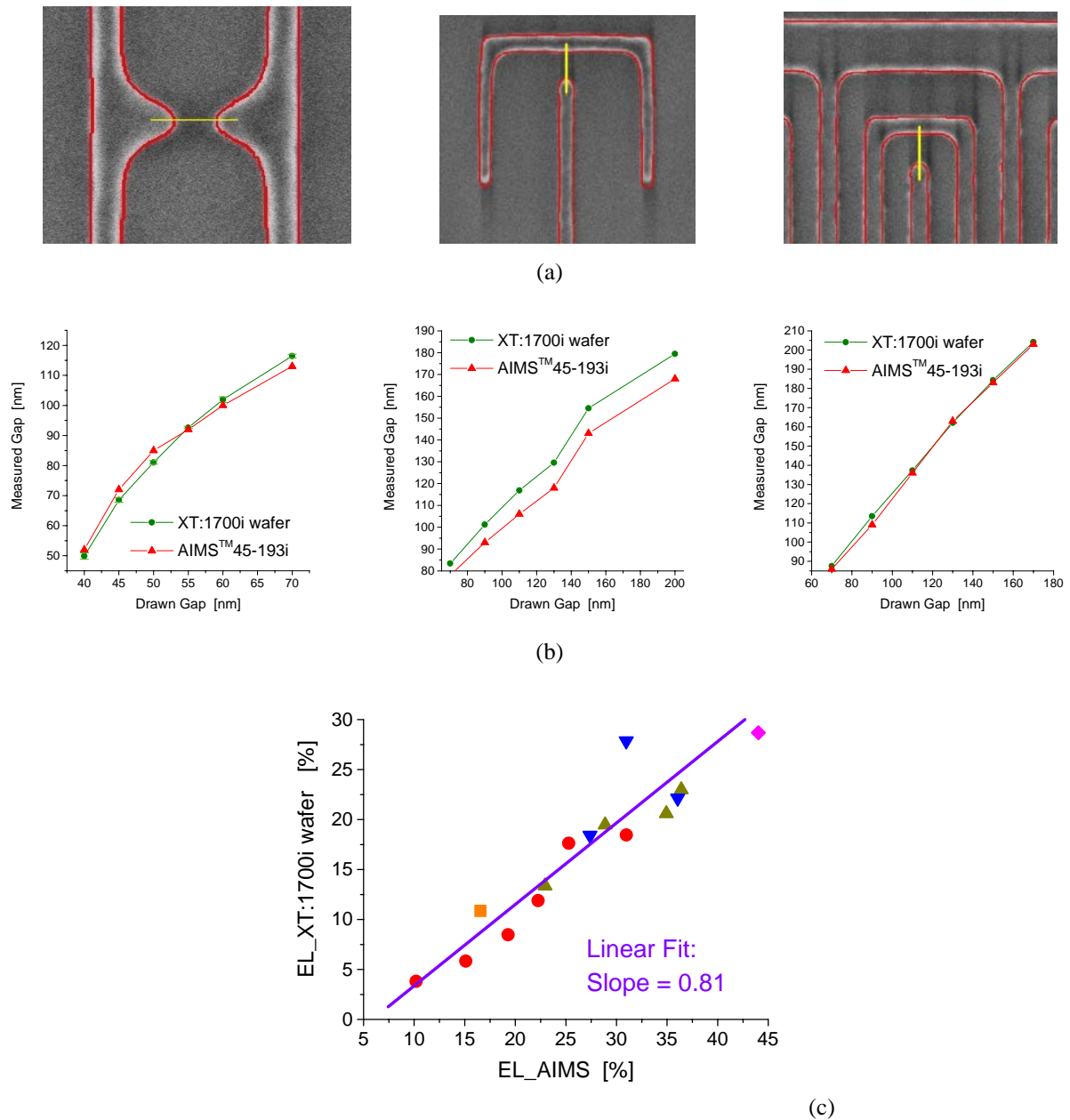


Fig. 10 Comparison of gap-measurements from AIMS™ 45-193i and XT:1700i wafers (NA = 1.20 Annular $\sigma = 0.96/0.72$ XY-polarized).

(a) Overlay of contours from the AIMS™ 45-193i images with SEM images from the printed wafers.

(b) Measured gap width and the bottom row the exposure latitude of this gap. The image threshold used for analyzing the AIMS™ 45-193i data was identical for all images (namely 0.213), and was chosen to match the width of one of the straight line segments of one of the 18 2D structures to the line-width measured from the wafer.

(c) Correlation plot between the maximum Exposure Latitude as measured from printed XT:1700i wafers vs. the AIMS™ values. (The different symbols refer to different gap- or line-structures within these 2D structures)

5. SUMMARY AND OUTLOOK

The newly developed AIMS™ 45-193i offers the possibility to operate in the so-called ‘scanner mode’ in which a ‘vector-effect emulation’ of the actually measured images is made that ‘converts’ them into a prediction of what the image-in-resist would look like in a hyper-NA wafer scanner.

This paper first presented experiments in which we tried to verify the validity of this ‘vector-effect emulation mode’, and we found it to be quite accurate. Next we explored the application of this ‘scanner mode’ for measurements of basic lithographic quantities like EL, MEF and through-focus performance of simple L/S structures, and compared the results to direct measurements of these quantities from wafers printed on the XT:1700i hyper-NA scanner at IMEC. We found that the AIMS™ 45-193i predicts the correct trends in all cases but not correct absolute values. The latter is in fact to be expected from the fact that the AIMS™ 45-193i analyses do not include resist-process nor thin-film effects. We obtained similar conclusions on an (initial) comparison for 2D structures. Does this mean that – after being used for more than a decade in the mask shops – the AIMS™ 45-193i could now also play a useful role in the wafer fab? We believe that is indeed the case, although more experiments would be required to further explore possible wafer-fab applications. In any case, from our work, we believe that AIMS™ 45-193i could be most useful when applied to 2D litho structures. Indeed, the lithographic behavior of 1D litho structures can be efficiently and accurately investigated with rigorous lithographic simulators. These have a reasonably high calculation throughput and incorporate mask-3D and resist effects, even though the mask is usually treated in an idealized way and accurate resist models are not easy to get. But the requirement (and cost) to actually build a mask before one can do AIMS™ 45-193i experiment would put it in an unfavorable position as a potential ‘competitor’ for lithography simulators for most 1D-related questions.

For 2D structures the situation is quite different, because lithographic simulators quickly run into run-time and memory-problems when the simulation area increases, and incorporating mask-3D effects (important for hyper-NA lithography) becomes quite unrealistic. The fact that the AIMS™ 45-193i captures through-focus image-intensities over a micron-size area makes it a natural tool to investigate or inspect the performance of 2D mask structures. One possible application would be to use the AIMS™ 45-193i as an ‘*OPC-defect inspection*’ tool: locations in the chip for which either exposure- or through-focus-performance is expected to be critical (e.g. locations that were flagged by OPC-inspection software) could be tried on the AIMS™ 45-193i prior to or in parallel with inspection of printed wafers. Data obtained from the AIMS™ 45-193i could also help identify why a certain location in the chip is not performing as expected. Alternative applications could possibly be defined for double-imaging or double-patterning applications where the AIMS™ 45-193i would allow to generate e.g. additional data on critical image-stitching locations. So while remaining a tool for inspecting reticle-defects, the AIMS™ 45-193i seems to have the potential to being used also for *inspecting ‘imaging-defects’*.

The usefulness of such imaging-related applications of the AIMS™ 45-193i would of course be further enhanced if the analyses could be extended to incorporate also the effect of the resist-process. This step is currently is not yet developed but could be a potential new development for the AIMS™ 45-193i software. It is perhaps useful to speculate on ways how this could be achieved. The most obvious way would be to add a resist-model step, after the ‘vector-effect emulation’ calculation, in the AIMS™ 45-193i software itself. Another way could be to build an interface between the AIMS™ 45-193i image-output and OPC-software packages⁶. OPC software uses calibrated models to make predictions of resist images from image-intensity data. So this type of software might be naturally suited to be combined with any system that can accurately measure such intensity data, while incorporating all effects of the actual mask (and not based on the assumption of an ideal mask only).

What the accuracy of such a combination would be for predicting absolute values of CDs, exposure latitude, through focus performance, OPE etc., is of course unknown at this point, as differences with the actual scanner will still remain (e.g. lens aberrations, stray-light performance, details of the illuminator, laser-bandwidth effects etc.) However, the AIMS™ tool has the ability to fully characterize the lithographic relevant optical behavior of the mask. Further studies would be needed to clarify all these issues, and could tell how much closer this brings us to mimicking the actual lithography process.

ACKNOWLEDGEMENTS

Jeroen Van de Kerckhove (IMEC) did a lot of essential work in preparing the measurements on the AIMS™ 45-193i and in the wafer CD-measurements. This study also benefited from discussions with Lieve Van Look, Joost Bekaert and Eric Hendrickx (IMEC). The authors also would like to thank Oliver Kienzle from Carl Zeiss SMS for strongly supporting this work and discussing the results.

REFERENCES

- ¹ TM: Trademark of Carl Zeiss.
- ² R.A. Budd et al., "Development and Application of a new tool for lithographic mask evaluation, the stepper equivalent Aerial Image Measurement System, AIMS", IBM J. Res. Develop. **41**(1,2) January / March 1997
- ³ A. Zibold et al., "First results for hyper NA scanner emulation from AIMS™45 – 193i", Photomask and Next-Generation Lithography Mask technology XIII (PMJ), Proc. of SPIE Vol. **6283** (2006) 628312-1
- ⁴ T. Scherübl, A.C. Dürr, K. Böhm, R. Birkner, R. Richter, E. Strössner, "Programmed defects study on masks for 45 nm immersion lithography using the novel AIMS™45-193i", 23rd European Mask and Lithography Conference (EMLC), Proc. of SPIE Vol. **6533** (2007) 653309-1
- ⁵ T. Konishi, Y. Kojima, V. Philipsen, P. Leunissen, L. Van Look, "Through-pitch and through-focus characterization of AAPSM for ArF immersion lithography", Proc. of SPIE Vol. **6281**, (2006)
- ⁶ OPC-software has already been used for automatic generation of AIMS™ inspection sites. See: G. Davis, S.Y. Choi, E.H. Chung, A. Seyfarth, H. van Doornmalen, E. Poortinga, "Automated aerial image based CD metrology initiated by pattern marking with photomask layout data", Photomask and Next-Generation Lithography Mask technology XIV (PMJ), Proc. of SPIE Vol. **6607** (2007) 60072A 1-10